

# Transformer-based stereo-aware 3D object detection from binocular images

Hanqing Sun, Yanwei Pang, *Senior Member, IEEE*, Jiale Cao, *Member, IEEE*, Jin Xie, and Xuelong Li, *Fellow, IEEE*

**Abstract**—Vision Transformers have shown promising progress in various object detection tasks, including monocular 2D/3D detection and surround-view 3D detection. However, when used in essential and classic stereo 3D object detection, directly adopting those surround-view Transformers leads to slow convergence and significant precision drops. We argue that one of the causes of this defect is that the surround-view Transformers do not consider the stereo-specific image correspondence information. In a surround-view system, the overlapping areas are small, and thus correspondence is not a primary issue. In this paper, we explore the model design of vision Transformers in stereo 3D object detection, focusing particularly on extracting and encoding the task-specific image correspondence information. To achieve this goal, we present TS3D, a Transformer-based Stereo-aware 3D object detector. In the TS3D, a Disparity-Aware Positional Encoding (DAPE) model is proposed to embed the image correspondence information into stereo features. The correspondence is encoded as normalized disparity and is used in conjunction with sinusoidal 2D positional encoding to provide the location information of the 3D scene. To extract enriched multi-scale stereo features, we propose a Stereo Reserving Feature Pyramid Network (SRFPN). The SRFPN is designed to reserve the correspondence information while fusing intra-scale and aggregating cross-scale stereo features. Our proposed TS3D achieves a 41.29% Moderate Car detection average precision on the KITTI test set and takes 88 ms to detect objects from each binocular image pair. It is competitive with advanced counterparts in terms of both precision and inference speed.

**Index Terms**—Stereo vision, 3D object detection, Transformer, positional encoding, feature pyramid.

## I. INTRODUCTION

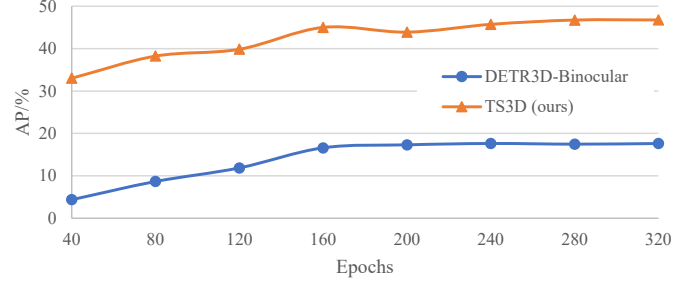
IMAGE correspondence information plays an essential role in 3D scene perception in stereo vision systems [1]–[3]. Image correspondence information, in the form of disparity or depth supervisions, is widely used in convolutional neural network (CNN) based stereo 3D object detection to prevent the stereo-based detector from converging to a monocular local minimum during training [4], [5]. Existing stereo 3D object detectors are divided into two categories based on the source of the image correspondence information: detectors with and without LiDAR-based image correspondence supervision.

Hanqing Sun, Yanwei Pang, and Jiale Cao are with the Tianjin Key Laboratory of Brain-Inspired Intelligence Technology, School of Electrical and Information Engineering, Tianjin University, Tianjin, China. (e-mail: {hqsun, pyw, conner}@tju.edu.cn).

Jin Xie is with the School of Big Data and Software Engineering, Chongqing University, Chongqing, China. (e-mail: xiejin@cqu.edu.cn).

Xuelong Li is with the School of Computer Science and School of Artificial Intelligence, Optics and Electronics (iOPEN), Northwestern Polytechnical University, Xi'an, China. (e-mail: li@nwpu.edu.cn).

Manuscript received April 24, 2023.



(a) Curves of Moderate validation AP of DETR3D-Binocular and TS3D

Method	Epochs	Mod.	Easy	Hard
DETR3D [17]-Binocular	320	17.61	29.95	13.69
TS3D (ours)	320	<b>46.75</b>	<b>70.50</b>	<b>35.48</b>

(b) KITTI validation set benchmarks of DETR3D-Binocular and our TS3D

Fig. 1. We adapt the Transformer-based surround-view 3D object detector DETR3D [17] to binocular detection, and name it DETR3D-Binocular. The DETR3D-Binocular and our TS3D are both trained on the KITTI train subset for 320 epochs. Their (a) Moderate validation AP during training are plotted and (b) the 3D detection APs are listed. DETR3D-Binocular converges to a poor 3D detection AP, whereas the Transformer-based TS3D can be trained to a superior performance.

The former [5]–[7], shortened as **Stereo-with-LiDAR**, generates ground-truth image correspondence information based on projected LiDAR point clouds, resulting in accurate yet sparse supervision, while The latter [8], [9], shortened as **Stereo-without-LiDAR**, does not rely on LiDAR point clouds to generate ground-truth image correspondence information. However, the pseudo ground-truths obtained by external stereo matching networks can provide inaccurate supervision in those methods [4], [10]. Some detectors in this category do not use explicit image correspondence supervision [11], [12]. Although Stereo-with-LiDAR detectors achieve higher detection precision, developing Stereo-without-LiDAR detectors is still essential as LiDAR devices may not always be affordable or available, such as in stereo endoscopes and traffic cameras.

Vision Transformers [13] has gained promising progress in 2D object detection [14]–[16], surround-view 3D object detection [17]–[19], and depth estimation [20]. However, for stereo 3D object detection in driving scenes, to the best of our knowledge, there have not been any public Transformer-based detectors in the literature.

An intuitive way to introduce vision Transformers into stereo 3D object detection is to adopt the above surround-view Transformer-based 3D detectors on the KITTI [21] dataset. To

achieve that, we train a binocular revision of the surround-view 3D object detector DETR3D [17], which is named DETR3D-Binocular. The validation AP curve of DETR3D-Binocular during training is shown in Fig. 1a as blue circles, and its evaluation indicators after training 320 epochs are listed in Fig. 1b. It can be seen that DETR3D-Binocular converges to a poor 3D detection performance, which can be compared neither to advanced CNN-based stereo 3D object detectors nor to the surround-view detection performance [22] of DETR3D.

We argue that the convergence problem is caused by a lack of image correspondence supervision in surround-view 3D object detection Transformers such as DETR3D, as well as in existing monocular-based and LiDAR-based 3D object detection Transformers. It is a fact that monocular images and LiDAR point clouds do not involve cross-view correspondence [23], [24]; and the overlapping area across images in a surround-view system is small [22]. Concerning the binocular vision system, however, the overlap areas between left and right images are large. The image correspondence information in the large overlap areas, as mentioned above, is key to decoding the 3D scene. Therefore, extracting and exploiting the image correspondence information in a Transformer-based model is a task-specific challenge of stereo 3D object detection.

In order to encode the image correspondence information into Transformers, and to build a Transformer-based stereo 3D object detector, we present TS3D, a Transformer-based Stereo-aware 3D object detector. The key novelties of the TS3D lie in its Disparity-Aware Positional Encoding (DAPE) and Stereo Reserving Feature Pyramid Network (SRFPN).

In detail, a deformable Transformer decoder [25] is introduced to decode multi-scale stereo features. In the decoder, the DAPE is designed to explicitly encode the correspondence information into the stereo features. DAPE composites normalized disparities and sinusoidal 2D positional encoding [25], thus simultaneously providing position information in both 2D image space and 3D scene. In addition to the DAPE, a Non-Parametric Anchor-Based Object Query (NPAQuery) scheme is introduced. Compared with the widely-used parametric query, NPAQuery does not introduce new learnable parameters as query embeddings, instead, it reuses the stereo features as a uniformly distributed query embedding in the 2D image space.

Encoder-wisely, the SRFPN is proposed to preserve image correspondence information and extract enriched multi-scale stereo features for the above Transformer decoder. Besides providing semantic information as done in existing feature pyramid networks [1], [2], [26], SRFPN reserves both local information in low-level features and correspondence information in stereo features. The resultant stereo feature pyramid is then aggregated by intra-scale and cross-scale fusion while respecting the disparity-wise definition of the stereo features.

Experiments on the KITTI dataset show that TS3D is an effective Transformer model for stereo 3D object detection, and it is competitive with existing CNN-based counterparts in terms of accuracy and efficiency. Consequently, our TS3D can encode the image correspondence information into the Transformer model, thus alleviate the above convergence problem. The validation AP curve of our TS3D is plotted in Fig. 1a as orange triangles, and its validation results are listed in

Fig. 1b. It is shown that after reserving and encoding the image correspondence information by the proposed SRFPN and DAPE respectively, the detection AP is greatly improved. To the best of our knowledge, the proposed TS3D is the first public Transformer-based stereo 3D object detector for driving scene in the literature.

The key contributions of this paper can be summarized as three-fold:

- (1) Towards introducing Transformer model into stereo 3D object detection, we present the Transformer-based Stereo-aware 3D object detector (TS3D). It is a Stereo-without-LiDAR detector and can extract and encode the image correspondence information from binocular images.
- (2) The Disparity-Aware Positional Encoding (DAPE) is designed to explicitly encode the image correspondence information into stereo features by reusing the disparity logits, thus providing the Transformer decoder with the 3D scene information.
- (3) A Stereo Reserving Feature Pyramid Network (SRFPN) is proposed, which reserves image correspondence information in both intra-scale and cross-scale feature fusion. It provides multi-scale stereo features that hold enriched detail and correspondence informations for the Transformer decoder.

## II. RELATED WORK

Existing stereo 3D object detectors are based on convolutional neural networks (CNN) and are reviewed following the taxonomy introduced in Sec. I. Representative Transformer-based 3D detectors for monocular images, LiDAR point clouds, and surround-view images are briefly introduced, and readers are encouraged to refer to [27] for a more thorough review on 3D vision Transformers. Existing feature pyramid networks are reviewed as well, which relates to our SRFPN.

Stereo-with-LiDAR 3D object detectors are trained with LiDAR-based image correspondence information. Pseudo-LiDAR [7], [28], [29] formulates the task as a cascade of disparity estimation and LiDAR-based 3D detection, therefore, the image correspondence information is explicitly used in the former step. OCSTereo [30] and IDA-3D [31] exploit the image correspondence information in an instance-aware manner, that is, disparities in foreground pixels are seen more importantly. ZoomNet [32] also generates instance-wise image correspondence, however, it adopts external 3D models to densify the instance-wise correspondence. DSGN [5], PLUMENet [33], and CDN [34] use the image correspondence information as auxiliary supervision to the detection supervision. LIGA-Stereo [35] distillates 3D voxel features extracted from the LiDAR-based correspondence information in a knowledge-distillation [36] manner.

Stereo-without-LiDAR detectors are trained without LiDAR-based image correspondence information. Some detectors in this category use external stereo matching algorithms to generate coarse image correspondence information. YOLOStereo3D [4] generates coarse disparity maps [37] and uses them as a multi-task supervision in parallel

with the detection supervision. Disp R-CNN [8] generates instance-wise disparities [38] and utilizes external 3D model to densify the instance-wise correspondence as done in ZoomNet. RT3DStereo [10] uses the estimated disparity map as an intermediate image correspondence supervision. Some detectors use image correspondence information in an implicit manner or ignore the correspondence. Stereo R-CNN [11] and TLNet [39] only uses the image correspondence information from the 3D object annotations. RTS3D [12] implicitly utilizes the correspondence by representing 3D scenes in a 4D feature-consistent embedding space.

The Transformer-based 2D object detector DETR [14] reformulates the 2D object detection as a collection prediction task and removes the anchor generation and Non-Maximum Suppression (NMS) processes, resulting in an end-to-end detector. DeformableDETR [25] introduces a deformable attention module, which only applies the multi-head attention mechanism at several learnable key locations around the reference point. It significantly reduces the computational cost of the DETR decoder and converges faster. The Transformer-based unary 3D object detector MonoDTR [23] utilizes auxiliary supervision to implicitly learn depth-aware features and a depth-aware Transformer to mine context and depth information from global features. MonoDETR [40] takes 3D object candidates as queries and introduces an attention-based depth encoder to encode depth embeddings. A depth cross-attention module is proposed to decode inter-query and query-scene interactions. The Transformer-based surround-view 3D object detector DETR3D [17] uses a CNN to extract unary features of each view and a DETR decoder to predict objects. PETR [18] extends DETR3D by generating a 3D coordinate grid in the camera frustum space and fusing the 3D coordinates with the 2D features. BEVFormer [19] generates object queries on the bird's eye view (BEV) and uses both spatial and temporal information. A spatial cross-attention module is proposed to extract BEV features from each view; A temporal self-attention module is designed to fuse historical BEV features. In addition to the obvious differences in input modalities comparing our TS3D with the above Transformer-based object detectors, two novel components, namely DAPE and SRFPN, are proposed to encode the image correspondence information into enriched stereo feature pyramids.

Feature Pyramid Network (FPN) [41] exploits the multi-level nature of CNNs to generate multi-scale features, so that the features of each level focus more on objects of the specific scale. FPN improves the detection performance of multi-scale 2D object detection. RetinaNet [42] makes use of more levels of the features than that used in FPN, resulting in higher detection precision at a lower computational cost. Original FPN fuses feature from lower-resolution to higher-resolution (*i.e.*, top-down), and PAFPN [43] adds an aggregation network from higher-resolution to lower-resolution features (bottom-up). ASFF [44] adaptively fuses multi-scale features and spatially filters information that conflicts across scales. BiFPN [45] designs a simple and efficient bidirectional FPN, in which a basic structure consisting of top-down and bottom-up paths is repeated to capture enriched multi-scale features. RFP [46] recursively reuses the FPN structure and

introduces Atrous Spatial Pyramid Pooling (ASPP) module as a connection module between two FPNs, which improves the performance of 2D object detection. The above feature pyramids are carefully designed for unary 2D object detection and do not consider the image correspondence nature of binocular images. As a result, they can be applied to generate unary feature pyramids in stereo 3D object detection, nevertheless, directly applying them in stereo features will destroy the latent image correspondence information and affect the accuracy of 3D object detection.

### III. METHODOLOGY

We elaborate on our TS3D in this section. The overall architecture is introduced in Sec. III-A. The proposed SRFPN (Sec. III-C) and Transformer decoder (Sec. III-B) result in an encoder-decoder pipeline. The DAPE is detailed in Sec. III-B1 as a novel component in the decoder.

#### A. Overall architecture of TS3D

The overall architecture of TS3D is illustrated in Fig. 2. Sequentially, TS3D takes binocular images as inputs (blue boxes in the figures denote left view, green denotes right), extracts unary features and stereo features, estimates disparities, decodes object features using a multi-scale deformable DETR decoder [25], and regresses and classifies 3D objects.

Two weight-sharing ResNets [47] + FPN [41] are used to **extract multi-scale unary features** from left and right input images respectively. Fig. 2 is a schematic diagram of a three-level multi-scale network. For simplicity and clarity, the left and right unary features are represented in a stacked manner (*i.e.*, the stacked blue and green boxes in Fig. 2). The upper half is the primary unary feature pyramid obtained by ResNet; the lower half is the enhanced unary feature pyramid obtained by FPN. The index of each feature level in both pyramids is denoted as  $l \in 1, 2, 3$ .

The above unary features are then fed into **Stereo Reserving Feature Pyramid Network (SRFPN)**. Both primary and enhanced unary feature pyramids are exploited to construct correlation-based cost volumes [48], resulting in primary and enhanced cost volume pyramids (shown as orange boxes in the second column of Fig. 2). Constructed cost volume pyramids are then referred to as stereo feature pyramids in the SRFPN. Subsequently, primary and enhanced stereo features from each level of the two pyramids are merged, in which the correspondence information is kept intact. The resultant stereo-reserving feature pyramid is then cross-scale aggregated in a bottom-up manner. Finally, enriched and aggregated multi-scale stereo features are obtained for subsequent disparity estimation and Transformer decoder.

A concise **disparity estimation** head (lower right corner of Fig. 2) is introduced to predict disparity maps from the lowest-resolution stereo feature in the above feature pyramid. Stereo features are convolved and upsampled to produce higher-resolution disparity maps. The disparity estimation is supervised by pseudo ground-truth generated by the BlockMatching algorithm [37], making the resultant TS3D a Stereo-without-LiDAR 3D object detector.

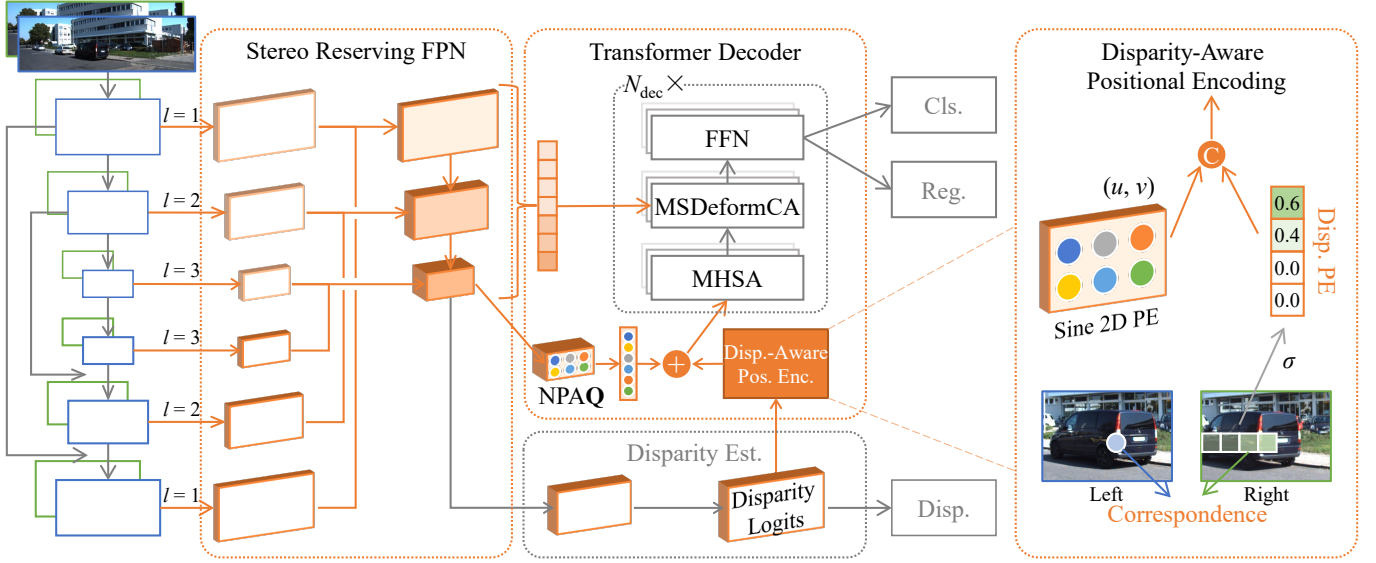


Fig. 2. The overall architecture of the Transformer-based Stereo-aware 3D object detector (TS3D). Sequentially, TS3D takes binocular images as inputs (blue boxes in the figures denote left view, green denotes right), extracts unary features, extracts stereo features using SRFPN (Stereo Reserving Feature Pyramid Network), estimates disparities, decodes object features using a multi-scale deformable DETR decoder [25], and regresses and classifies 3D objects. The DAPE (Disparity-Aware Positional Encoding) elaborated on the right is used to explicitly encode image correspondence information for detection.

The **Transformer decoder** consists of Multi-Head Self-Attention layers [14] (shortened as MHSA in Fig. 2), Multi-Scale Deformable Cross-Attention layers [25] (MSDeformCA), and Feed-Forward Networks (FFNs). The last feature tensor for disparity regression is termed disparity logits and is used as the input of our DAPE. The generated positional encoding of the 3D scene is summed with the query of each layer in the Transformer decoder. The lowest-resolution features in the above feature pyramid are convolved to generate embeddings of the NPAQuery. In addition to the DAPE and NPAQuery, the multi-scale stereo features extracted by SRFPN are exploited as keys and values of the MSDeformCA layers. The above procedure including MHSA, MSDeformCA, and FFN is collectively referred to as a decoder layer. The Transformer decoder is a cascade of  $N_{\text{dec}}$  decoding layers, in which the object queries are refined step-by-step. During training, 3D objects are classified and regressed under ground-truth supervision after each decoder layer; During inference, only predictions from the last layer are taken as the final 3D object detection results.

The **detection head** [4] consists of two sub-heads of classification and regression, both of which are predicted at  $1/16$  resolution. For the classification head,  $K + 1$  scores are predicted for  $K$ -class objects, where the extra class denotes the background class. Offsets *w.r.t.* anchor boxes are regressed by the regression head. The offset is defined as a 13-dimensional vector: the projected 2D bounding box  $(u_{2D}, v_{2D}, w_{2D}, h_{2D})$ , projected 3D object center  $(u_{3D}, v_{3D})$ , object distance  $z$ , object 3D size  $(w, h, l)$ , and object orientation  $(\sin 2\alpha, \cos 2\alpha, c_\alpha)$ .

### B. Transformer decoder

DeformableDETR [25] introduces a Multi-Scale Deformable Cross-Attention (MSDeformCA) layer in the DETR decoder [14]. We first briefly review the key processes of

MSDeformCA as preliminary knowledge in this section. Flattened multi-scale features are used as the key and value of MSDeformCA, and object embeddings extracted by MHSA are used as queries. A reference point is first extracted from an object query; then, MSDeformCA is applied to regress  $n_{\text{points}}$  offset points around it. The Multi-Head Cross-Attention (MHCA) mechanism is only applied to those points, which not only reduces the computational cost and GPU memory footprint, but also speeds up the training convergence. Therefore, MSDeformCA can be applied to multi-scale features since its computational cost are controllable.

Despite the success of MSDeformCA in 2D object detection, directly applying it in stereo 3D object detection still leads to a difficult convergence during model training. To speed up the convergence of such a model, we introduce image correspondence information to stereo features. Image correspondence information can ensure that the model makes full use of the stereo features, instead of falling into the local minimum of unary 3D object detection [5]. Towards that end, a Transformer decoder is designed as shown in Fig. 2. The main difference between our decoder and a DeformableDETR decoder is Disparity-Aware Positional Encoding (Sec. III-B1) and Non-Parametric Anchor-Based Object Query (Sec. III-B2).

As shown in Fig. 2, Disparity-Aware Positional Encoding is aimed to explicitly encode image correspondence information based on disparity logits. The generated positional encoding holds the 3D location information in the scene. It is fed into the decoder as an addition to the NPAQuery, thus introducing 3D information into the Transformer decoder. The multi-scale stereo features (refer to Sec. III-C) are flattened and concatenated (in Fig. 2, a small square represents the feature vector of a pixel in the stereo feature, and varying saturations represent features from different scales). The resultant

2D feature matrix is used as the multi-scale key/value in MSDeformCA. The downsampling ratios of the feature maps of the three resolutions relative to the input image are 4, 8, and 16, respectively, that is,  $\mathbf{x}^l \in \mathbb{R}^{\frac{W}{2^{l+1}} \times \frac{H}{2^{l+1}} \times C_{\text{dec}}}$ , where  $l \in \{1, 2, 3\}$ ,  $C_{\text{dec}}$  denotes the dimension of feature vectors in the decoder. Only the lowest-resolution stereo features are reused in the NPAQuery, which maintains the inference speed while accelerating the training convergence. For other hyperparameters in MSDeformCA, we use  $N_{\text{dec}} = 4$  decoder layers, each layer is of  $M = 8$  heads, and each MSDeformCA samples  $K = 4$  offset points.

1) *Disparity-Aware Positional Encoding (DAPE)*: Positional encoding is an important component in vision Transformers [13], [18], [49]. The sinusoidal 2D positional encoding [14] is widely used in existing Transformer-based 2D object detectors.

However, positional encodings for 2D object detection lack 3D scene information; positional encodings for unary, point cloud, and surround-view 3D object detection ignore the correspondence information between binocular images. Therefore, DAPE is proposed to explicitly encode the image correspondence information into stereo features based on disparities, thus enabling the decoder to perceive the 3D information of the scene and objects.

We reuse the disparity logits in the disparity estimation head. The disparity prediction at position  $(u, v)$  on the disparity map  $\hat{\mathbf{M}}$  is regressed using SoftArgMax [1] by the disparity logits  $\mathbf{x}_{\hat{\mathbf{M}}}$ :

$$\hat{\mathbf{M}}(u, v) = \text{SoftArgMax}(\mathbf{x}_{\hat{\mathbf{M}}}(u, v, :)), \quad (1)$$

where  $\mathbf{x}_{\hat{\mathbf{M}}} \in \mathbb{R}^{W \times H \times C_{\text{disp}}}$ , and  $C_{\text{disp}} < C_{\text{dec}}$ . We proposed to reuse the Softmax normalized version of  $\mathbf{x}_{\hat{\mathbf{M}}}$  as the probability distribution of disparity at  $(u, v)$ , thus introducing the correspondence information into the decoder. Formally, it can be given as

$$\text{PE}_{\text{disp}}(\mathbf{x}_{\hat{\mathbf{M}}}; u, v, :) = \sigma(\mathbf{x}_{\hat{\mathbf{M}}}(u, v, :)), \quad (2)$$

where  $\sigma(\cdot)$  denotes Softmax normalization. The DAPE is a concatenation of the sinusoidal 2D and the disparity-related encoding defined by Eq. (2), that is,

$$\text{PE}_{\text{DA}}(\mathbf{x}_{\hat{\mathbf{M}}}; u, v, :) = [\text{PE}_{\text{sine}}(u, v, :), \text{PE}_{\text{disp}}(\mathbf{x}_{\hat{\mathbf{M}}}; u, v, :)], \quad (3)$$

where  $\text{PE}_{\text{disp}}(\mathbf{x}_{\hat{\mathbf{M}}}; u, v, :)$  is a  $C_{\text{disp}}$ -dimensional vector,  $\text{PE}_{\text{sine}}(u, v, :)$  is re-defined as a  $(C_{\text{dec}} - C_{\text{disp}})$ -dimensional vector, so  $\text{PE}_{\text{DA}}(\mathbf{x}_{\hat{\mathbf{M}}}; u, v, :)$  is a  $C_{\text{dec}}$ -dimensional vector, which can be summed directly with the object query.

DAPE is added to the NPAQuery to provide explicit image correspondence and 3D position information for stereo features:

$$\mathbf{Q} = \mathbf{x}_q + \text{PE}_{\text{DA}}(\mathbf{x}_{\hat{\mathbf{M}}}), \quad (4)$$

where  $\mathbf{x}_q \in \mathbb{R}^{\frac{W}{16} \times \frac{H}{16} \times C_{\text{dec}}}$  is the NPAQuery elaborated in Sec. III-B2, and  $\mathbf{x}_q$  and  $\text{PE}_{\text{DA}}(\mathbf{x}_{\hat{\mathbf{M}}})$  are reshaped to  $\mathbb{R}^{(\frac{W}{16} \cdot \frac{H}{16}) \times C_{\text{dec}}}$ .

It can be seen from Eqs. (2) and (3) that the DAPE not only encodes 2D information in the 2D image space but also explicitly encodes the correspondence information of

binocular images. It is suitable for locating the projection of 3D object center points and bounding boxes in 2D images; The encoded image correspondence information is guided by stereo features, thus is suitable for regressing depths and sizes of 3D objects in 3D space.

2) *Non-Parametric Anchor-Based Object Query (NPA-Query)*: Existing methods assign a best-matching object query to each object. When the number of positive samples is small (as that in KITTI), few object queries can be trained in each iteration, resulting in less training efficiency. As a consequence, it is difficult for the model to learn useful 3D object statistics. In addition, in order to make object queries cover the entire 3D scene, existing 3D object detectors usually generate dense 3D grids. Therefore, the number of object queries becomes large to ensure that it can cover the entire 3D space, which makes the training harder to converge.

To alleviate that problem while ensuring the object query able to cover the entire 3D space, we reuse the lowest-resolution features in the pyramid (Sec. III-C). The feature map can cover the entire 2D image space, and with the 3D information provided by the proposed DAPE, it can cover the 3D space. The NPAQuery does not depend on learnable parameters as do in [29], [50], thus we term it a non-parametric object query. Using higher-resolution feature maps can cover the 3D space more densely, but it also leads to a significant increase in the computational cost. In terms of query quantity and coverage, the lowest-resolution stereo feature is a compromise.

As mentioned above, the lowest-resolution feature  $\mathbf{x}^{l=3} \in \mathbb{R}^{\frac{W}{16} \times \frac{H}{16} \times C_{\text{x}}^3}$ . The number of feature channels is convolved to  $C_{\text{dec}}$  by a  $1 \times 1$  convolution, and the resulting tensor is denoted as  $\mathbf{x}_q \in \mathbb{R}^{\frac{W}{16} \times \frac{H}{16} \times C_{\text{dec}}}$ , which is used as object embeddings. After flattening, the query becomes  $\mathbf{x}_q \in \mathbb{R}^{1440 \times C_{\text{dec}}}$ , which is equivalent to 1440 object queries:  $N_q = \frac{W}{16} \times \frac{H}{16} = 1440$ . Although this number is much higher than empirical values in 2D object detection [25], it is comparable to the values in surround-view 3D object detection [18].

Because the coordinate correspondence between the NPA-Query and the 2D image space is clear, we therefore directly generate the reference point coordinates according to this correspondence. Such design makes it possible to exploit anchor prior [4], which is commonly used in CNN-based detectors. During training, targets are assigned *w.r.t.* 2D IoUs (Intersection over Union) between anchor boxes and ground-truth boxes. If an IoU is greater than a preset foreground threshold  $\tau_{\text{fg}}$ , the corresponding anchor is assigned as a matching positive sample; On the contrary, if an IoU is smaller than a preset background threshold  $\tau_{\text{bg}}$ , the anchor is assigned as a negative sample.

### C. Stereo Reserving Feature Pyramid Network

The above Transformer decoder can decode 3D object attributes from stereo features so as to complete the 3D object detection. In order to provide the Transformer decoder with more discriminative stereo features and to embed rich detail and correspondence information into the stereo features, we propose Stereo Reserving Feature Pyramid Network (SRFPN).



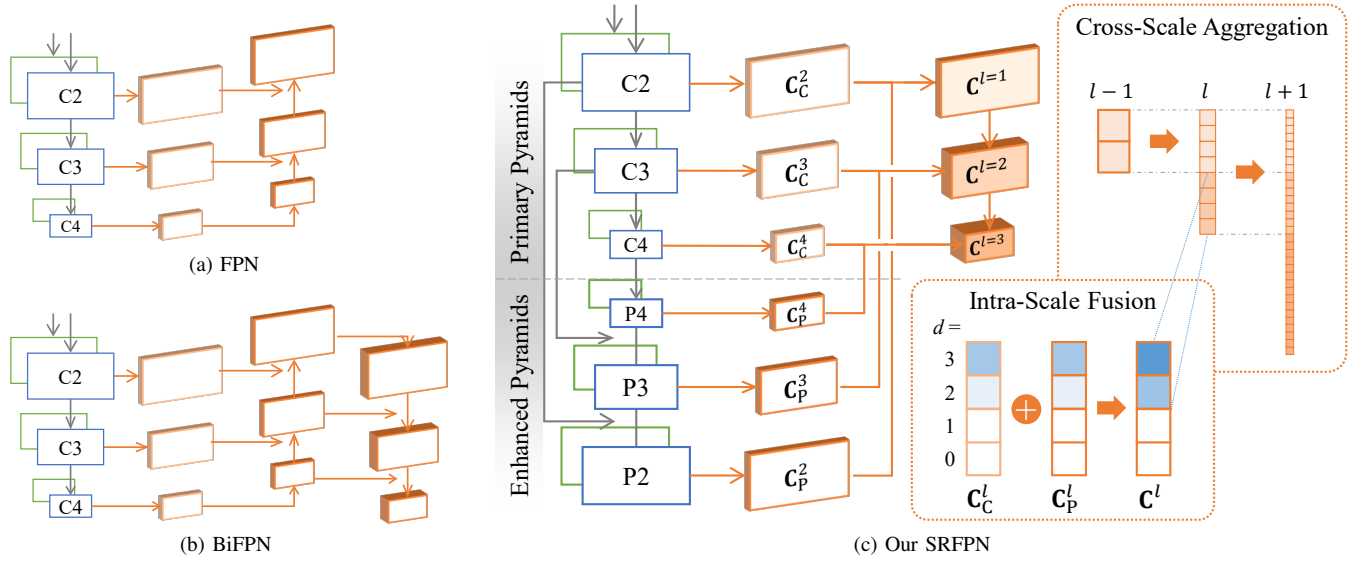


Fig. 3. Comparing (a) FPN [41] and (b) BiFPN [45] with the proposed (c) Stereo Reserving Feature Pyramid Network (SRFPN). FPN consists of a top-down path and BiFPN introduces an additional bottom-up path. Our SRFPN utilizes the FPN to extract multi-scale unary features, and a six-level three-scale cost volume pyramid is constructed from the unary features. Intra-Scale Fusion is performed where disparity dimensions are of identical definition, thus the stereo features are summed accordingly; Cross-Scale Aggregation is performed where disparity dimensions are of different definitions, thus the stereo features are expended and concatenated with the lower-resolution feature. The image correspondence information is therefore reserved.

The feature pyramid network can extract multi-scale features in a neural network model, which is suitable for addressing the scale variation problem in object detection tasks. In stereo 3D object detection, on the one hand, unary features suffer from scale variation as does in 2D object detection, making the feature pyramid network one of the crucial designs. On the other hand, stereo features contain image correspondence information and have clear physical meanings. Directly using existing feature pyramid networks for 2D object detection will destroy the 3D information, since those ignore the intra-scale and cross-scale relationships of stereo features. Existing feature pyramids are constructed on either unary features or stereo features: the former cannot perform information interaction across scales of stereo features; the latter suffers from the low quality of the initial cost volumes.

To address those problems, we propose the SRFPN, which consists of three parts (three columns of features as shown in Fig. 3c). The first column presents the unary feature pyramid. As described in Sec. III-A, the upper part is the primary pyramid (C2–C4) and the lower part is the enhanced pyramid (P2–P4). Six levels of paired unary features with three levels of resolutions are used to construct a six-level correlation-based cost volume pyramid [9], [48] (orange rectangles in the second column in the figure). The upper three levels in the figure are obtained from primary unary features, which contain rich detailed information; the lower three levels are from enhanced unary features, which contain more semantic information. The primary and enhanced stereo features are fused according to their resolutions. Knowing the fact that the channel dimensions of identical resolution stereo features have consistent physical meanings, those two feature tensors are directly summed. The resulting multi-scale stereo features contain rich details and correspondence information. In addition, the features of the lowest resolution will be reused as NPAQuery. In order to get

better object embeddings, the higher-resolution stereo features are step-by-step fused with lower-resolution features [4] (the downward arrows in the third column of Fig. 3c). Each scale focuses on objects within the range of the receptive field [41], therefore, the cross-scale fusion in this paper is completed by channel expansion and concatenation. Finally, the lowest-resolution stereo features with the largest number of feature channels are obtained and reused in NPAQuery.

Then in primary unary features, the left unary feature  $\mathbf{x}_{L,C}^{l+1}$  and the right unary feature  $\mathbf{x}_{R,C}^{l+1}$  construct primary 3D cost volumes by

$$\mathbf{C}_C^{l+1} = \text{CV}_{3D}(\mathbf{x}_{L,C}^{l+1}, \mathbf{x}_{R,C}^{l+1}), \quad (5)$$

where  $\text{CV}_{3D}(\cdot, \cdot)$  correlation based cost volume [48],  $\mathbf{x}_{L,C}^{l+1}, \mathbf{x}_{R,C}^{l+1} \in \mathbb{R}^{\frac{W}{2^{l+1}} \times \frac{H}{2^{l+1}} \times C}$ ,  $\mathbf{C}_C^{l+1} \in \mathbb{R}^{\frac{W}{2^{l+1}} \times \frac{H}{2^{l+1}} \times \frac{D}{2^{l+1}}}$ ,  $D$  denotes the maximum disparity value. Similarly, the enhanced unary features,  $\mathbf{x}_{L/R,P}^{l+1}$  construct enhanced 3D cost volumes. It can be observed that  $\mathbf{C}_C^{l+1}$  and  $\mathbf{C}_P^{l+1}$  are of identical definition along the disparity dimension so that summation will not change the physical meaning of that dimension. Therefore, the initial stereo feature of the  $l$ -th scale in the third column of Fig. 3c is

$$\mathbf{C}_{\text{init}}^l = \mathbf{C}_C^{l+1} + \mathbf{C}_P^{l+1}, \quad (6)$$

$\mathbf{C}_{\text{init}}^l \in \mathbb{R}^{\frac{W}{2^{l+1}} \times \frac{H}{2^{l+1}} \times \frac{D}{2^{l+1}}}$  is kept. However, definitions of the disparity dimension across scales are not the same. In order not to destroy the physical meaning of each scale, the cross-scale fusion can be expressed recursively as

$$\begin{aligned} \mathbf{C}^l &:= \text{Concat}[\mathbf{C}^l, \text{Conv}_{3 \times 3, s, 2}(\mathbf{C}^{l-1})], \\ \mathbf{C}^1 &= \mathbf{C}_{\text{init}}^1, \end{aligned} \quad (7)$$

where  $\text{Conv}_{3 \times 3, s, 2}(\cdot)$  denotes a  $3 \times 3$  convolutional layer with a stride of 2.

Additionally, Figs. 3a and 3b respectively showcase using FPN [41] and BiFPN [45] for extracting multi-scale stereo features. It can be seen from Fig. 3a that the feature fusion direction of FPN is top-down, *i.e.*, using high-level features to supplement semantic information for low-level. However, the lowest-resolution stereo features play a vital role in NPAQuery, so we choose to use higher-resolution features to supplement the detailed information of lower-resolution features. In this way, it tends to cause a lack of semantic information on high-resolution features. Therefore, an hourglass-shaped SRFPN is designed, where the bottom high-resolution features are enhanced by rich semantic information. The BiFPN (Fig. 3b) introduces top-down and bottom-up multi-scale feature fusion. Although it can enrich the final multi-scale stereo features, its cross-scale fusion method will destroy the image correspondence information of different scales.

#### IV. EXPERIMENTS

##### A. Experimental setup

The experiments are conducted on the KITTI dataset [21]. In the ablation experiments, the data split is consistent with that of [51] and the evaluation index is obtained on its validation subset. We report all difficulty levels (Easy, Moderate, Hard) of 3D Car detection AP (Average Precision) as benchmarking indicators. In the experiments in Sec. IV-C, the entire training set is used during training, and the prediction results are calculated by the KITTI server. Detection APs of three difficulty levels of 3D, BEV, and 2D Car detection tasks are reported. Among them, Moderate 3D Car detection AP is the main evaluation index in this paper, which is placed as the first column of AP in each table and marked in *italics*.

The TS3D model is implemented based on PyTorch 1.10.0 [52] and Python 3.7.11. During training, four NVIDIA Quadro P6000 GPUs are used with CUDA 11.1.74 and CuDNN 8.0.5 installed.

In the ablation experiments, ResNet-34 [47] is used as the backbone. The disparity dimensions of multi-scale cost volumes are set to 24, 48, and 96, respectively, from highest-resolution to lowest-resolution. The experiments on KITTI test set use ResNet-50 as the backbone, the disparity dimensions are 48, 48, and 96, respectively. The rest hyperparameters remain unchanged.

During the training process, 8 training samples are input on each GPU for each iteration, resulting in an equivalent batchsize of 32 on four GPU parallel training. The resolution of the input RGB image is uniformly cropped to  $W = 1280$ ,  $H = 288$ . Training samples are randomly horizontally flipped with a probability of 0.5.

##### B. Ablation study

Ablation study is performed on the KITTI validation set, and experimental results are shown in Tab. I. The first row shows the result of directly using the Transformer-based surround-view 3D object detector DETR3D [17] to train on KITTI. The training process is unstable and the detection accuracy is poor. The DAPE (second row) is used in conjunction with NPAQuery to enrich the stereo features, and the

TABLE I  
ABLATION STUDY ON THE KITTI VALIDATION SET.

Transformer	DAPE + NPAQuery	SRFPN	<i>Mod.</i>	Easy	Hard
✓			17.61	29.95	13.69
✓	✓		45.59	70.98	34.71
✓	✓	✓	<b>46.76</b>	<b>70.90</b>	<b>35.94</b>
		✓	44.06	68.94	33.24
		✓	<b>45.27</b>	<b>70.69</b>	<b>35.77</b>

TABLE II  
COMPARING OUR DISPARITY-AWARE POSITIONAL ENCODING (DAPE)  
WITH EXISTING POSITIONAL ENCODINGS.

PE	<i>Mod.</i>	Easy	Hard
w/o PE	44.63	69.76	33.88
Sine2D PE	45.17	70.82	34.38
Disparity PE	43.54	67.18	32.95
DAPE	<b>45.59</b>	<b>70.98</b>	<b>34.71</b>

Moderate AP is greatly improved by 27.98 p.p. (percentage points), and other indicators are improved as well. Finally, the SRFPN (third row) is introduced to further introduce the detail and correspondence information into stereo features, which improves the Moderate detection AP by 1.17 p.p. As a comparison, we also implement the SRFPN on the CNN-based YOLOStereo3D [4] (fourth row), and the results are given in the fifth row. Compared with baseline results on the fourth row, using SRFPN gains an improvement in detection AP (1.21 p.p.), proving that SRFPN is also effective in CNNs. Thanks to its image correspondence information reserving design, the extracted stereo features are enriched and more discriminative.

1) *Design of positional encoding*: The DAPE is compared with the widely-used sinusoidal 2D positional encoding and disparity-only encoding. The results are listed in Tab. II. Specifically, the sinusoidal 2D positional encoding in the table is a fixed embedded 2D positional encoding. The disparity-only positional encoding is a simple way to explicitly encode disparity information into stereo features. First, use ArgMax to find the candidate disparity on the disparity map, and then set the positional embedding of the disparity value index position to 1, and the other parts set to 0. This scheme is similar to the one-hot encoding. Although it can introduce matching information into stereo features, it neither considers the 2D locations of the image nor can it obtain sub-pixel-level disparity. No positional encodings are introduced in the first row of Tab. II, which serves as a comparison baseline. The second row shows that using sinusoidal 2D positional encoding can introduce location information and the detection AP is improved (0.54 p.p.), however, it does not introduce image correspondence information. The disparity-only positional encoding in the third row explicitly introduces the correspondence information. Results have proved that considering only the correspondence information while ignoring the 2D location information is harmful to 3D object detection. The DAPE (last row) of this paper considers both 2D location information and sub-pixel-level stereo matching information but does not enforce the discretization of disparity. It uses the latent correspondence information in stereo features to

TABLE III  
COMPARING OUR STEREO RESERVING FEATURE PYRAMID NETWORK (SRFPN) WITH EXISTING FEATURE PYRAMIDS.

Pyramid	Aggregation	Mod.	Easy	Hard
FPN [41]	Top-down	34.49	51.92	26.61
BiFPN [45]	Top-down & bottom-up	44.19	67.37	33.72
SRFPN	Stereo reserving & bottom-up	<b>46.76</b>	<b>70.90</b>	<b>35.94</b>

guide the disparity-aware positional embedding. DAPE is a learnable binocular 3D positional encoding, in contrast to the fixed sinusoidal 2D positional encoding. Experiments show that DAPE outperforms the above three schemes and can provide suitable 3D spatial information for stereo 3D object detection.

2) *SRFPN compared with existing FPNs*: In this subsection, a variety of existing feature pyramid networks are implemented to extract multi-scale stereo features. A comparison of those and our SRFPN can be seen in Tab. III. The first row shows the result of applying FPN [41] to extract multi-scale stereo features (detailed in Sec. III-C). The results show that the direct use of FPN will lead to a significant decline in APs. The reason, as mentioned above, is that these methods do not consider the physical meaning of the disparity dimension of stereo features. Many FPNs are aimed to enrich features of higher-resolution (*i.e.*, top-down aggregation), which is not compatible with the idea of reusing lowest-resolution features in this paper. BiFPN [45] (Sec. III-C) uses high-level features to supplement the semantic information of low-level features, and then aggregates features to high-level features from the bottom up. Therefore, the results in the second row show that the fusion of multi-scale stereo features based on BiFPN can significantly improve the detection AP compared with the above three existing pyramid networks. The last row in Tab. III shows the detection AP of the model based on our SRFPN. Results prove that SRFPN is more suitable for extracting multi-scale stereo features and can retain crucial 3D scene information, providing the Transformer decoder with more discriminative object queries.

3) *The number of decoder layers and the usage of intermediate supervision*: This subsection gradually changes the number of decoding layers in the Transformer decoder, that is,  $N_{\text{dec}} \in \{2, 4, 6, 8\}$ . The first row of Tab. IV is the detection AP of the baseline model without Transformer decoder (*i.e.*,  $N_{\text{dec}} = 0$ ). When the decoder is added without additional supervision (third row), a significant drop in detection AP can be observed. Conversely, by adding appropriate supervision (Sec. III-A) at each decoding layer, the detection AP can be improved regardless of the number of decoder layers. Continuing to increase the number of decoder layers can improve detection AP, however, it requires longer training time. We set  $N_{\text{dec}} = 4$  in the final model.

### C. Comparison with existing methods

The performance of our TS3D on the KITTI test set is given in this subsection. The evaluation indicators of three difficulty levels (Easy, Moderate, and Hard) including 3D, BEV, and 2D object detection tasks are displayed in the last row of Tab. V.

TABLE IV  
THE IMPACT OF THE NUMBER OF DECODER LAYERS AND INTERMEDIATE SUPERVISIONS.

Decoder #Layer	Inter. Superv.	Mod.	Easy	Hard
$N_{\text{dec}} = 0$		45.27	70.69	35.77
$N_{\text{dec}} = 2$	✓	45.54	70.71	35.87
$N_{\text{dec}} = 4$		42.79	63.68	32.68
$N_{\text{dec}} = 4$	✓	46.76	<b>70.90</b>	35.94
$N_{\text{dec}} = 6$	✓	<b>46.79</b>	70.34	35.44
$N_{\text{dec}} = 8$	✓	46.71	70.49	<b>36.01</b>

As a first Transformer-based stereo 3D object detector in the literature at the time of writing, TS3D achieves competitive detection results compared with advanced CNN-based detectors. In the KITTI test set Moderate difficulty, the 3D Car detection AP of TS3D reaches 41.29%, which is generally the same as that of the latest existing methods without LiDAR-based stereo matching supervision, *i.e.*, YOLOStereo3D [4] in ICRA 2021. Compared with other models in the table, TS3D is based on the vision Transformer model. Compared with the first part of the table, that is, using LiDAR-based stereo matching supervisions during training, TS3D does not rely on LiDAR to provide disparity annotations during training. Compared with other detectors that do not rely on LiDAR in the second part, in addition to the difference of the neural network model, the method of this paper has the following differences. From the perspective of multi-scale features, TLNet [39] and RT3DStereo [10] use single-scale feature maps; Whereas TS3D proposes SRFPN to generate multi-scale feature maps. Stereo R-CNN [11] only extracts multi-scale unary features, uses single-scale features in the 3D object RoI head; TS3D uses SRFPN modules in stereo features, extracts unary and stereo two pyramids of multi-scale features. RTS3D [12], YOLOStereo3D, Disp R-CNN [8] also use the feature pyramid for both unary features and stereo features; but do not use a method similar to the SRFPN to fuse multi-scale stereo features. From the perspective of additional informations required for training, in addition to 3D object annotations, TS3D requires a stereo matching algorithm to generate pseudo-ground-truth disparity maps; RT3DStereo relies on semantic segmentation annotations; RTS3D takes coarse 3D bounding boxes as input and gradually optimizes the detection results to achieve high-quality 3D object detection; Disp R-CNN needs to use external 3D models to generate more accurate pseudo point clouds for candidate objects. From the perspective of detection pipelines, Stereo R-CNN requires complex post-processing steps to obtain a more accurate 3D object bounding box after predicting the 3D bounding box; TS3D only uses 2D NMS [54] as the post-processing step. Stereo R-CNN, TLNet, and Disp R-CNN are two-stage algorithms [54]; whereas TS3D is a single-stage detector [55].

Tab. V also lists the external dependencies and runtime of the existing methods that do not rely on LiDAR-based stereo matching supervisions. Among them, Disp R-CNN and S3D [9] are higher than TS3D in Moderate 3D Car detection AP, however, the detection speed of the two is slower, respectively 0.42 seconds and 0.67 seconds. TS3D



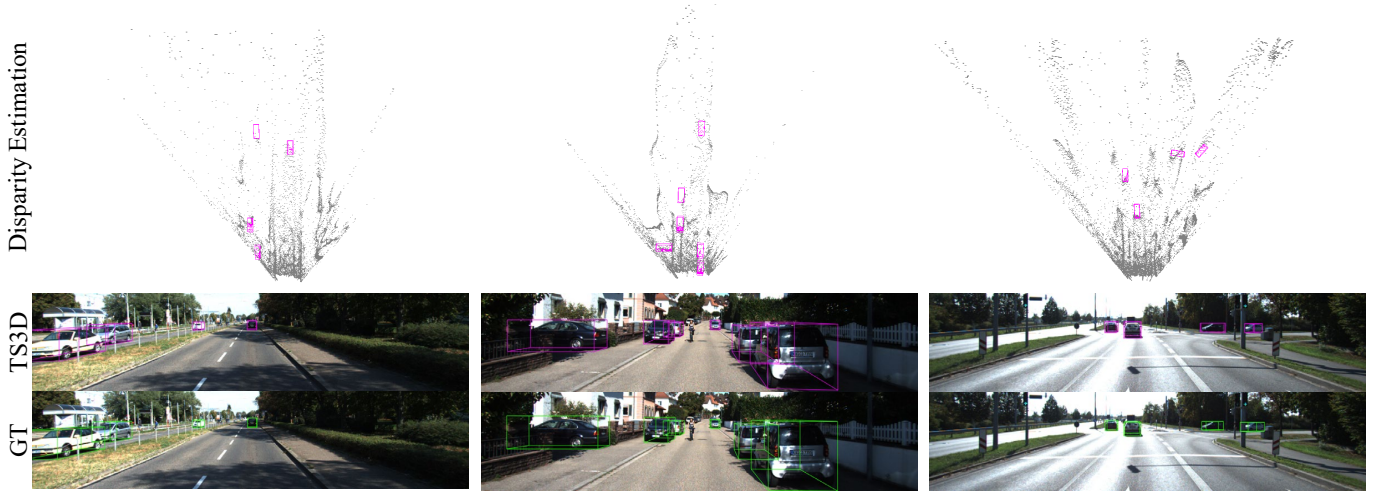


Fig. 4. Visualization of three detection results of our TS3D on the KITTI validation set, one column each. From top to bottom of each sample: inverse-projection of disparity estimation and 3D detection (pink), left image with projected 3D detection (pink), and left image with 3D ground-truth boxes (green).

TABLE V

RESULTS ON THE KITTI TEST SET OF OUR TS3D. IT IS COMPETITIVE WITH ADVANCED CNN-BASED DETECTORS IN TERMS OF BOTH AP AND SPEED.

Model – Category	3D Car Detection			Runtime	
	Method	Mod.	Easy	Hard	(sec.) Dependency
<b>CNN – Stereo-with-LiDAR</b>					
PL: AVOD [7]	34.05	54.53	28.25	0.40	LiDAR point cloud
OCStereo [30]	37.60	55.15	30.25	0.35	LiDAR point cloud, instance segmentation
ZoomNet [32]	38.64	55.98	30.97	0.35	LiDAR point cloud, instance segmentation
PL++: P-RCNN [28]	42.43	61.11	36.99	0.40	LiDAR point cloud
E2E-PL: P-RCNN [29]	43.90	64.80	38.10	0.40	LiDAR point cloud
CDN: PL++ [34]	44.86	64.31	38.11	0.40	LiDAR point cloud
Disp R-CNN (velo) [8]	45.78	68.21	37.73	0.42	LiDAR point cloud, instance segmentation, 3D model
DSGN [5]	52.18	73.50	45.14	0.67	LiDAR point cloud
CGStereo [53]	53.58	74.39	46.50	0.57	LiDAR point cloud, semantic segmentation
CDN: DSGN [34]	54.22	74.52	46.36	0.60	LiDAR point cloud
LIGA-Stereo [35]	64.66	81.39	57.22	0.35	LiDAR point cloud
<b>CNN – Stereo-without-LiDAR</b>					
TLNet [39]	4.37	7.64	3.74	—	—
RT3DStereo [10]	23.28	29.90	18.96	0.08	Pseudo disparity GT, semantic segmentation
Stereo R-CNN [11]	30.23	47.58	23.72	0.30	—
RTS3D [12]	37.38	58.51	31.12	0.04	—
YOLOStereo3D [4]	41.25	65.68	30.42	0.08	Pseudo disparity GT
Disp R-CNN [8]	43.27	67.02	36.43	0.42	Pseudo disparity GT, instance segmentation, 3D model
<b>Transformer – Stereo-without-LiDAR</b>					
DETR3D [17]-Binocular	17.61	29.95	13.69	—	—
TS3D	41.29	64.61	30.68	0.09	Pseudo disparity GT

takes only 0.09 seconds to detect from a pair of binocular images. In addition, TS3D merely relies on the pseudo-ground-truth of stereo matching, while Disp R-CNN requires instance segmentation supervision and 3D models during training.

We also visualizes three detection results of TS3D on the KITTI validation set (Fig. 4, one column each). The first row visualizes the inverse-projection of disparity map predicted by TS3D and detected 3D bounding boxes (pink); The second row illustrates the projection of detected 3D bounding boxes onto the left image. The last row shows the projection of 3D ground-truth boxes on the left image. In the first column in Fig. 4, the shadow of trees on the side of the road is a challenge for image-based object detectors, and the distant vehicle ahead is of relatively small-scale. Thanks to the explicitly embedded

rich details and correspondence information in multi-scale stereo features and Transformer decoders, TS3D can alleviate the problems of scale variation and shadow defects. The second column shows a roadside parking scene on a narrow road. In addition to the detected roadside cars of various scales, TS3D is also able to detect the car parked vertically on the left. The third column showcases the detection of distant cars. All four cars are detected, however, the right two cars are of erroneous orientations due to their small scale.

## V. CONCLUSIONS

Vision Transformer is making progress in various fields of computer vision, and the performance of Transformer model

in many fields is comparable to or exceeds that of the state-of-the-art CNN model. We have proposed a Transformer-based Stereo-aware 3D object detector (TS3D), which has successfully applied the Transformer model to the stereo 3D object detection task by designing Disparity-Aware Positional Encoding (DAPE) and Stereo Reserving Feature Pyramid Network (SRFPN). The image correspondence and 2D location informations have been explicitly encoded into object queries by DAPE, providing the decoder with the spatial information of the 3D scene. The SRFPN has been designed to provide the Transformer decoder with enriched multi-scale features and object embeddings. In the fusion process, SRFPN has reserved the image correspondence information in the stereo features; In the cross-scale aggregation, the complementary image correspondence information across scales has been aggregated, and eventually, the stereo feature pyramid with enriched details and correspondence information has been obtained.

Experiments on the KITTI dataset have shown that TS3D is an effective Transformer model for stereo 3D object detection, which has been competitive with advanced methods of CNN-based models, achieving 41.29% of the test set Moderate Car detection AP. Ablation experiments have demonstrated the effectiveness of the proposed DAPE and SRFPN. The TS3D could hopefully serve as a baseline for future research on the Transformer model for stereo 3D object detection.

#### ACKNOWLEDGMENTS

This work was partially supported by the National Key R&D Program of China under Grant 2022ZD0160400, the National Key R&D Program of China under Grant 2018AAA0102800, the Tianjin Science and Technology Program under Grant 19ZXZNGX00050, and the Tianjin Natural Science Foundation under Grant JCQNJC00420.

#### REFERENCES

- [1] J.-R. Chang and Y.-S. Chen, "Pyramid stereo matching network," in *IEEE Conference on Computer Vision and Pattern Recognition*. Salt Lake City, UT, USA: IEEE, 2018, pp. 5410–5418.
- [2] H. Yi, Z. Wei, M. Ding, R. Zhang, Y. Chen, G. Wang, and Y.-W. Tai, "Pyramid multi-view stereo net with self-adaptive view aggregation," in *European Conference on Computer Vision*. Glasgow, UK: Springer International Publishing, 2020, pp. 766–782.
- [3] J. Nie, Y. Pang, J. Xie, J. Pan, and J. Han, "Stereo Refinement Dehazing Network," *IEEE Transactions on Circuits and Systems for Video Technology*, vol. 32, no. 6, pp. 3334–3345, 2022.
- [4] Y. Liu, L. Wang, and M. Liu, "YOLOStereo3D: A step back to 2D for efficient stereo 3D detection," in *IEEE International Conference on Robotics and Automation*. Xi'an, China: IEEE, 2021, pp. 13 018–13 024.
- [5] Y. Chen, S. Liu, X. Shen, and J. Jia, "DSGN: Deep stereo geometry network for 3D object detection," in *IEEE Conference on Computer Vision and Pattern Recognition*. Seattle, WA, USA: IEEE, 2020, pp. 12 533–12 542.
- [6] A. Gao, Y. Pang, J. Nie, Z. Shao, J. Cao, Y. Guo, and X. Li, "ESGN: Efficient stereo geometry network for fast 3D object detection," *IEEE Transactions on Circuits and Systems for Video Technology*, pp. 1–1, 2022.
- [7] Y. Wang, W.-L. Chao, D. Garg, B. Hariharan, M. Campbell, and K. Q. Weinberger, "Pseudo-LiDAR from visual depth estimation: Bridging the gap in 3D object detection for autonomous driving," in *IEEE Conference on Computer Vision and Pattern Recognition*. Long Beach, CA, USA: IEEE, 2019, pp. 8437–8445.
- [8] J. Sun, L. Chen, Y. Xie, S. Zhang, Q. Jiang, X. Zhou, and H. Bao, "Disp R-CNN: Stereo 3D object detection via shape prior guided instance disparity estimation," in *IEEE Conference on Computer Vision and Pattern Recognition*. Seattle, WA, USA: IEEE, 2020, pp. 10 545–10 554.
- [9] H. Sun, J. Cao, and Y. Pang, "Semantic-aware self-supervised depth estimation for stereo 3D detection," *Pattern Recognition Letters*, vol. 167, pp. 164–170, 2023.
- [10] H. Königshof, N. O. Salscheider, and C. Stiller, "Realtime 3D object detection for automated driving using stereo vision and semantic information," in *IEEE Intelligent Transportation Systems Conference*. Auckland, New Zealand: IEEE, 2019, pp. 1405–1410.
- [11] P. Li, X. Chen, and S. Shen, "Stereo R-CNN based 3D object detection for autonomous driving," in *IEEE Conference on Computer Vision and Pattern Recognition*. Long Beach, CA, USA: IEEE, 2019, pp. 7636–7644.
- [12] P. Li, S. Su, and H. Zhao, "RTS3D: Real-time stereo 3D detection from 4D feature-consistency embedding space for autonomous driving," in *AAAI Conference on Artificial Intelligence*. Online: AAAI, 2021, pp. 1930–1939.
- [13] A. Dosovitskiy, L. Beyer, A. Kolesnikov, D. Weissenborn, X. Zhai, T. Unterthiner, M. Dehghani, M. Minderer, G. Heigold, S. Gelly, J. Uszkoreit, and N. Houlsby, "An image is worth 16x16 words: Transformers for image recognition at scale," in *International Conference on Learning Representations*, Online, 2021.
- [14] N. Carion, F. Massa, G. Synnaeve, N. Usunier, A. Kirillov, and S. Zagoruyko, "End-to-end object detection with transformers," in *European Conference on Computer Vision*, ser. Lecture Notes in Computer Science. Glasgow, UK: Springer International Publishing, 2020, pp. 213–229.
- [15] L. Dai, H. Liu, H. Tang, Z. Wu, and P. Song, "AO2-DETR: Arbitrary-Oriented Object Detection Transformer," *IEEE Transactions on Circuits and Systems for Video Technology*, pp. 1–1, 2022.
- [16] P. Zhen, X. Yan, W. Wang, T. Hou, H. Wei, and H.-B. Chen, "Toward Compact Transformers for End-to-End Object Detection With Decomposed Chain Tensor Structure," *IEEE Transactions on Circuits and Systems for Video Technology*, vol. 33, no. 2, pp. 872–885, 2023.
- [17] Y. Wang, V. Guizilini, T. Zhang, Y. Wang, H. Zhao, and J. Solomon, "DETR3D: 3D Object Detection from Multi-view Images via 3D-to-2D Queries," in *Conference on Robot Learning*. London, UK: PMLR, 2021, pp. 180–191.
- [18] Y. Liu, T. Wang, X. Zhang, and J. Sun, "PETR: Position Embedding Transformation for Multi-view 3D Object Detection," in *European Conference on Computer Vision*. Tel Aviv, Israel: Springer Nature Switzerland, 2022, pp. 531–548.
- [19] Z. Li, W. Wang, H. Li, E. Xie, C. Sima, T. Lu, Y. Qiao, and J. Dai, "BEVFormer: Learning Bird's-Eye-View Representation from Multi-camera Images via Spatiotemporal Transformers," in *European Conference on Computer Vision*. Tel Aviv, Israel: Springer Nature Switzerland, 2022, pp. 1–18.
- [20] Z. Li, X. Liu, N. Drenkow, A. Ding, F. X. Creighton, R. H. Taylor, and M. Unberath, "Revisiting stereo depth estimation from a sequence-to-sequence perspective with Transformers," in *IEEE International Conference on Computer Vision*. Online: IEEE, 2021, pp. 6197–6206.
- [21] A. Geiger, P. Lenz, and R. Urtasun, "Are we ready for autonomous driving? The KITTI vision benchmark suite," in *IEEE Conference on Computer Vision and Pattern Recognition*. Providence, RI, USA: IEEE, 2012, pp. 3354–3361.
- [22] H. Caesar, V. Bankiti, A. H. Lang, S. Vora, V. E. Liong, Q. Xu, A. Krishnan, Y. Pan, G. Baldan, and O. Beijbom, "nuScenes: A multimodal dataset for autonomous driving," in *IEEE Conference on Computer Vision and Pattern Recognition*. Seattle, WA, USA: IEEE, 2020, pp. 11 618–11 628.
- [23] K.-C. Huang, T.-H. Wu, H.-T. Su, and W. H. Hsu, "MonoDTR: Monocular 3D object detection with depth-aware transformer," in *IEEE Conference on Computer Vision and Pattern Recognition*. New Orleans, LA, USA: IEEE, 2022, pp. 4002–4011.
- [24] H. Sheng, S. Cai, Y. Liu, B. Deng, J. Huang, X.-S. Hua, and M.-J. Zhao, "Improving 3D Object Detection with Channel-wise Transformer," in *IEEE International Conference on Computer Vision*. Montreal, QC, Canada: IEEE, 2021, pp. 2723–2732.
- [25] X. Zhu, W. Su, L. Lu, B. Li, X. Wang, and J. Dai, "Deformable DETR: Deformable transformers for end-to-end object detection," in *International Conference on Learning Representations*, Online, 2021.
- [26] Z. Wu, X. Wu, X. Zhang, S. Wang, and L. Ju, "Semantic stereo matching with pyramid cost volumes," in *IEEE International Conference on Computer Vision*. Seoul, Korea: IEEE, 2019, pp. 7483–7492.

- [27] J. Lahoud, J. Cao, F. S. Khan, H. Cholakkal, R. M. Anwer, S. Khan, and M.-H. Yang, "3D Vision with Transformers: A Survey," *Arxiv*, vol. 2208.04309, 2022.
- [28] Y. You, Y. Wang, W.-L. Chao, D. Garg, G. Pleiss, B. Hariharan, M. Campbell, and K. Q. Weinberger, "Pseudo-LiDAR++: Accurate depth for 3D object detection in autonomous driving," in *International Conference on Learning Representations*, New Orleans, LA, USA, 2019.
- [29] R. Qian, D. Garg, Y. Wang, Y. You, S. Belongie, B. Hariharan, M. Campbell, K. Q. Weinberger, and W.-L. Chao, "End-to-end Pseudo-LiDAR for image-based 3D object detection," in *IEEE Conference on Computer Vision and Pattern Recognition*. Seattle, WA, USA: IEEE, 2020, pp. 5881–5890.
- [30] A. D. Pon, J. Ku, C. Li, and S. L. Waslander, "Object-centric stereo matching for 3D object detection," in *IEEE International Conference on Robotics and Automation*. Paris, France: IEEE, 2020, pp. 8383–8389.
- [31] W. Peng, H. Pan, H. Liu, and Y. Sun, "IDA-3D: Instance-depth-aware 3D object detection from stereo vision for autonomous driving," in *IEEE Conference on Computer Vision and Pattern Recognition*. Seattle, WA, USA: IEEE, 2020, pp. 13 012–13 021.
- [32] Z. Xu, W. Zhang, X. Ye, X. Tan, W. Yang, S. Wen, E. Ding, A. Meng, and L. Huang, "ZoomNet: Part-aware adaptive zooming neural network for 3D object detection," in *AAAI Conference on Artificial Intelligence*. New York City, NY, USA: AAAI, 2020, pp. 12 557–12 564.
- [33] Y. Wang, B. Yang, R. Hu, M. Liang, and R. Urtasun, "PLUMENet: Efficient 3D object detection from stereo images," in *IEEE International Conference on Intelligent Robots and Systems*. Online: IEEE, 2021, pp. 3383–3390.
- [34] D. Garg, Y. Wang, B. Hariharan, M. Campbell, K. Weinberger, and W.-L. Chao, "Wasserstein distances for stereo disparity estimation," in *Advances in Neural Information Processing Systems*. Online: Curran Associates, Inc., 2020, pp. 22 517–22 529.
- [35] X. Guo, S. Shi, X. Wang, and H. Li, "LIGA-Stereo: Learning LiDAR geometry aware representations for stereo-based 3D detector," in *IEEE International Conference on Computer Vision*. Online: IEEE, 2021, pp. 3153–3163.
- [36] G. Hinton, O. Vinyals, and J. Dean, "Distilling the knowledge in a neural network," in *Advances in Neural Information Processing Systems: Deep Learning Workshop*. Montreal, QC, Canada: MIT Press, 2014.
- [37] G. Bradski, "The OpenCV library," *Dr. Dobbs's Journal of Software Tools*, 2000.
- [38] K. He, G. Gkioxari, P. Dollár, and R. B. Girshick, "Mask R-CNN," in *IEEE International Conference on Computer Vision*. Venice, Italy: IEEE, 2017, pp. 2980–2988.
- [39] Z. Qin, J. Wang, and Y. Lu, "Triangulation learning network: From monocular to stereo 3D object detection," in *IEEE Conference on Computer Vision and Pattern Recognition*. Long Beach, CA, USA: IEEE, 2019, pp. 7607–7615.
- [40] R. Zhang, H. Qiu, T. Wang, Z. Guo, X. Xu, Y. Qiao, P. Gao, and H. Li, "MonoDETR: Depth-guided Transformer for Monocular 3D Object Detection," *Arxiv*, vol. 2203.13310, 2022.
- [41] T.-Y. Lin, P. Dollár, R. B. Girshick, K. He, B. Hariharan, and S. J. Belongie, "Feature pyramid networks for object detection," in *IEEE Conference on Computer Vision and Pattern Recognition*. Honolulu, HI, USA: IEEE, 2017, pp. 936–944.
- [42] T.-Y. Lin, P. Goyal, R. B. Girshick, K. He, and P. Dollár, "Focal loss for dense object detection," in *IEEE International Conference on Computer Vision*. Venice, Italy: IEEE, 2017, pp. 2999–3007.
- [43] S. Liu, L. Qi, H. Qin, J. Shi, and J. Jia, "Path aggregation network for instance segmentation," in *IEEE Conference on Computer Vision and Pattern Recognition*. Salt Lake City, UT, USA: IEEE, 2018, pp. 759–768.
- [44] S. Liu, D. Huang, and Y. Wang, "Learning Spatial Fusion for Single-Shot Object Detection," *Arxiv*, vol. 1911.09516, 2019.
- [45] M. Tan, R. Pang, and Q. V. Le, "EfficientDet: Scalable and efficient object detection," in *IEEE Conference on Computer Vision and Pattern Recognition*. Seattle, WA, USA: IEEE, 2020, pp. 10 778–10 787.
- [46] S. Qiao, L.-C. Chen, and A. Yuille, "DetectoRS: Detecting Objects with Recursive Feature Pyramid and Switchable Atrous Convolution," in *IEEE Conference on Computer Vision and Pattern Recognition*. Nashville, TN, USA: IEEE, 2021, pp. 10 208–10 219.
- [47] K. He, X. Zhang, S. Ren, and J. Sun, "Deep residual learning for image recognition," in *IEEE Conference on Computer Vision and Pattern Recognition*. Las Vegas, NV, USA: IEEE, 2016, pp. 770–778.
- [48] N. Mayer, E. Ilg, P. Häusser, P. Fischer, D. Cremers, A. Dosovitskiy, and T. Brox, "A large dataset to train convolutional networks for disparity, optical flow, and scene flow estimation," in *IEEE Conference on Computer Vision and Pattern Recognition*. Las Vegas, NV, USA: IEEE, 2016, pp. 4040–4048.
- [49] Y. Liu, J. Yan, F. Jia, S. Li, Q. Gao, T. Wang, X. Zhang, and J. Sun, "PETRv2: A Unified Framework for 3D Perception from Multi-Camera Images," *Arxiv*, vol. 2206.01256, 2022.
- [50] F. Li, H. Zhang, S. Liu, J. Guo, L. M. Ni, and L. Zhang, "DN-DETR: Accelerate DETR Training by Introducing Query DeNoising," in *IEEE Conference on Computer Vision and Pattern Recognition*. New Orleans, LA, USA: IEEE, 2022, pp. 13 609–13 617.
- [51] X. Chen, H. Ma, J. Wan, B. Li, and T. Xia, "Multi-view 3D object detection network for autonomous driving," in *IEEE Conference on Computer Vision and Pattern Recognition*. Honolulu, HI, USA: IEEE, 2017, pp. 6526–6534.
- [52] A. Paszke, S. Gross, F. Massa, A. Lerer, J. Bradbury, G. Chanan, T. Killeen, Z. Lin, N. Gimelshein, L. Antiga, A. Desmaison, A. Kopf, E. Yang, Z. DeVito, M. Raison, A. Tejani, S. Chilamkurthy, B. Steiner, L. Fang, J. Bai, and S. Chintala, "PyTorch: An imperative style, high-performance deep learning library," in *Advances in Neural Information Processing Systems 32*, H. Wallach, H. Larochelle, A. Beygelzimer, F. d'Alché-Buc, E. Fox, and R. Garnett, Eds. Vancouver, Canada: Curran Associates, Inc., 2019, pp. 8024–8035.
- [53] C. Li, J. Ku, and S. L. Waslander, "Confidence guided stereo 3D object detection with split depth estimation," in *IEEE International Conference on Intelligent Robots and Systems*. Las Vegas, NV, USA: IEEE, 2020, pp. 5776–5783.
- [54] S. Ren, K. He, R. Girshick, and J. Sun, "Faster R-CNN: Towards real-time object detection with region proposal networks," in *Advances in Neural Information Processing Systems*, ser. NIPS'15. Montreal, QC, Canada: MIT Press, 2015, pp. 91–99.
- [55] W. Liu, D. Anguelov, D. Erhan, C. Szegedy, S. Reed, C.-Y. Fu, and A. C. Berg, "SSD: Single Shot MultiBox Detector," in *European Conference on Computer Vision*. Amsterdam, The Netherlands: Springer, 2016, pp. 21–37.